Available online at www.sciencedirect.com
SCIENCE DIRECT
Journal of Power Sources 157 (2006) 688–694
JOURNAL OF POWER SOURCES
www.elsevier.com/locate/jpowsour

Effect of components in electrodes on sintering characteristics of $Ce_{0.9}Gd_{0.1}O_{1.95}$ electrolyte in intermediate-temperature solid oxide fuel cells during fabrication

Masashi Mori [a,*], Eisaku Suda [b], Bernard Pacaud [b], Keiichiro Murai [c], Toshihiro Moriga [c]

[a] *Materials Science Research Laboratory, Central Research Institute of Electric Power Industry, 2-6-1 Nagasaka, Yokosuka, Kanagawa 240-0196, Japan*
[b] *R&D Department, Anan Kasei Co., Ltd., 210-51 Ohgata, Anan, Tokushima 774-0022, Japan*
[c] *Faculty of Engineering, The University of Tokushima, 2-1 Minami-Josanjima, Tokushima 770-8506, Japan*

Received 20 November 2005; received in revised form 9 January 2006; accepted 23 January 2006
Available online 24 February 2006

Abstract

The effects of anode and cathode components on solid-state reaction and sintering characteristics of $Ce_{0.9}Gd_{0.1}O_{1.95}$ (CGO) electrolyte were investigated in the temperature range from 900 to 1200 °C. The solubility limit of components in the anode was <4 mol% for $1/2Fe_2O_3$, <1 mol% for NiO, and <3 mol% for CuO. The solubility limit of components in the cathode was <4 mol% for $1/2La_2O_3$, <4 mol% for SrO, and <1 mol% for $1/3Co_3O_4$. A small amount of addition of Fe_2O_3, Co_3O_4 or CuO remarkably enhanced the sintering characteristics of the CGO nanopowder. NiO, La_2O_3 or SrO addition lowered. In the case of the mixture of the CGO and $La_{0.6}Sr_{0.4}CoO_3$, enhancement of sintering characteristics of the CGO and no reaction products were observed. From scanning electron microscopy observation, the sintered CGO samples with Fe_2O_3 showed the feature by solid-state sintering mechanism. For the CGO with CuO, the samples showed the trace of liquid-phase sintering. The samples of CGO with Co_3O_4 included large grains, which seem to relate to cobalt vapor from the cobalt oxide particles.

Keywords: IT-SOFC; Cerium oxide; Nanopowder; Sintering; Reaction

1. Introduction

Recently, there has been a growing interest in the realization of intermediate-temperature solid oxide fuel cells (SOFC) with an operating temperature of 500–600 °C [1]. In this temperature range, there arises a remarkable lowering of oxide-ion conduction in an electrolyte in addition to a lowering of catalytic activity of electrodes. When CeO_2-based oxides with a fluorite-type structure are compared with ZrO_2-based ones, they showed much higher oxide-ion conductivities, and thus are expected to be candidates for the electrolyte of the SOFC. The conductivities at the intermediate temperatures, however, are not enough as the electrolyte. Thus, its thickness of the electrolyte is desired to be as thin as possible, for example, the thickness is less than 10 μm. The thin electrolyte sheet with thickness of ∼10 μm is hard to handle during the SOFC fabrication process. On the other hand, the electrodes with thick wall are required so that voltage losses due to the internal resistance resulting from the small current path area and the long current paths are reduced [2]. From the reasons above, in the intermediate-temperature SOFC, a development of electrode-supported cells, where the electrode-substrate supports the thin electrolyte layer and provides the mechanical strength of the cell, is necessary.

Since the electrolyte must be gastight, it is said that an acceptable relative density of impervious ceramic electrolyte is greater than 94% [3]. Quite recently, Nada et al. [4] indicated by AC impedance measurement that the bulk and grain boundary resistances of the $Ce_{0.8}Gd_{0.2}O_{1.9}$ electrolyte at the intermediate-temperatures have a tendency to decrease with increasing its density. In particular, there was a significant difference of electrical conductivity between sintered samples with 94% and 96% of theoretical density at 500 °C in air; 3.9×10^{-3} S cm^{-1} for sintered sample with relative density of 94%, and 5.2×10^{-3} S cm^{-1} for the sample with relative density of 96%. These data suggest that the relative density of the electrolyte should be greater than 96% in view of

* Corresponding author. Tel.: +81 46 856 2121; fax: +81 46 856 5571.
E-mail address: masashi@criepi.denken.or.jp (M. Mori).

0378-7753/$ – see front matter © 2006 Elsevier B.V. All rights reserved.
doi:10.1016/j.jpowsour.2006.01.062

electrical conductivity. In this paper, relative densities greater than 96% is used as an indication of appropriate electrolyte in the SOFC.

A sintering process at a rather high temperature is required to density the electrolyte. For the electrode-supported type cells, the co-firing fabrication process in which the electrolyte layer and electrode-substrate are fired together at the high temperature, cannot be avoided. During this high-temperature heat-treatment process, the components in the electrodes would diffuse into the electrolyte. For the stabilized zirconia, the sintering behavior and the oxide-ion conductivity of the electrolyte would be strongly affected by the components [5,6]. Therefore, the effect of the components on sintering of Ce-based electrolyte is also important. In addition, in some cases, such a high-temperature heat-treatment causes a degradation in the performance of the cathode or anode, for example, the formation of poorly conductive compounds at the interface between the electrode and electrolyte, and the loss of porosity of electrodes [7,8].

In order to prevent the degradation of the electrolyte and electrodes, the $Ce_{0.9}Gd_{0.1}O_{1.95}$ (CGO) nanopowders with high sintering characteristics have been developed using a newly-devised heat-treatment process in the coprecipitation method [9]. For this nanopowder, its relative densities greater than 94% can be achieved at temperatures greater than 1050 °C; the conventional powder can be sintered at temperatures greater than 1300 °C. Since the nanopowder has high sintering characteristics, there is a possibility that it has a peculiarly high chemical reactivity with electrodes of the SOFC. Generally, $La_{1-x}Sr_xCoO_3$-based perovskites are said to be a candidate for cathodes of the intermediate-temperature SOFC [10,11]. For the anode materials, Fe–, Ni–, and Cu–CGO cermets are candidates [12,13], and these cermets are Fe_2O_3–, NiO–, and CuO–CGO composites during the SOFC fabrication. In this paper, we studied the solid-state reaction of the CGO nanopowder with high sintering characteristics and components (La_2O_3, SrO, Co_3O_4, Fe_2O_3, NiO, and CuO) in electrodes of the intermediate-temperature SOFC, and discussed the effects of the components on sintering characteristics of the CGO nanopowder.

2. Experimental

The low-temperature sinterable CGO nanopowder was basically synthesized using the conventional coprecipitation method [9]: the metal nitrate aqueous solutions as starting materials, $Ce(NO_3)_3$ (99.9%, Rhodia, France) and $Gd(NO_3)_3$ (99.9%, Rhodia, France), were used. Concentrations of aqueous solutions of $Ce(NO_3)_3$ (ca. 2.5 mol L^{-1}), and $Gd(NO_3)_3$ (ca. 2.0 mol L^{-1}) were mixed in a selected proportion and were then poured into a water solution of NH_4HCO_3 (extra pure regent, Wako Pure Chem. Ltd., Japan). A large difference between the new and conventional coprecipitation methods is that the new method includes the pre-filtration heat-treatment process. For the new method, the homogeneous precipitate obtained by the conventional coprecipitation method was stirred at 80 °C for 3 h before the filtration. The precipitate collected by the filtration was dried and calcined at 700 °C for 5 h in air. Then, the exact compositions of the calcined powders were confirmed by inductively coupled plasma (ICP) analysis (Seiko Instruments Inc., SPS-3000). For the calcined CGO powder, it was confirmed by the transmission electron microscopy that the primary particles are all nanometer-sized particles and their size is approximately 20 nm diameter on average [9]. The main impurity in the CGO powders was 3 ppm for CaO and 1 ppm for Fe_2O_3. No impurities for silicon oxide and alumina, which have an influence on the sintering characteristics [14], were observed.

In order to clarify the solubility limits of components in the electrodes and the effect of the components on sintering characteristics of the CGO nanopowder, the samples were prepared using the CGO nanopowder and the oxides (M = La_2O_3, SrO, Co_3O_4, Fe_2O_3, NiO, CuO, 99.9%, High Purity Chem., Japan) via the solid-state technique. For La_2O_3, it was used after preheating at 1500 °C for 1 h. The particle size of starting materials is 0.19 μm for CGO and 1–2 μm for the oxides. For the solubility limit test and sintering characteristics, the CGO were mixed with the oxides in the region of 0.5–12 mol% oxide by Al_2O_3 mortar. The prepared powders were pressed into tablets of 20 mm diameter × 2 mm thickness under a pressure of 100 MPa. These samples, $(CGO)_{1-x}(MO)_x$, were then heated at selected temperatures with a heating/cooling rate of 200 °C h^{-1} in air. All the samples were analyzed by powdered X-ray diffractometry (XRD) (18 kW, Mac Science, Japan, M18XHF^{22}) using monochromated Cu Kα radiation and a scintillation detector. A scanning rate of 0.02° s^{-1} was used. Density of the sintered samples was determined from observed values of size and weight of the samples. Relative density was derived using the theoretical value determined from the experimental lattice parameters and unit formula. The shrinkage ratio of the CGO tablets with the oxides was determined as $(L_1 - L_2)/L_1$, where L_1 and L_2 are initial and final length, respectively.

Thermogravimetry and differential thermal analysis (TG-DTA) measurements for the CGO with the oxides were carried out using Mac Science TG-DTA 5000S equipment in air at a heating/cooling rate of 5 °C min^{-1}. Microanalysis of the dense sintered samples was carried out using a JEOL scanning electron microscope (SEM; JSM-T200).

3. Results and discussion

The solubility limit of each oxide into CGO was determined by an appearance of peaks of the oxides and reaction products except fluorite oxides, and a change of lattice parameters of CGO. After heating at 1200 °C, the CGO crystallized in a cubic fluorite unit $a = 5.4151$ (4) Å, $V = 158.79$ Å^3 and $z = 4$ (Space group Fm3m, No. 225). Fig. 1 shows the lattice parameters of CGO nanopowder heated with the components (NiO, Fe_2O_3 or CuO) in the anode at 1200 °C for 20 h in air as a function of content of the oxides. The closed symbols represent the samples with two phases. No reaction products were observed for all samples. With increasing addition of the oxides, the lattice parameters of the CGO increased and then showed the constant value. It was concluded that the solubility limit was <1 mol% for NiO, ≤4 mol% for 1/2Fe_2O_3 and <3 mol% for CuO. Table 1 summarizes the ionic radii of the oxides, the solubility limits of the oxides into the CGO nanopowder.

Table 1
Ionic radii of the oxides, solubility limits of the oxides into CGO, phase changes of the oxides, and effects of addition of the oxide on sintering characteristics of CGO nanopowder

Oxides	Ionic valence in fluorite	Ionic radius (ppm)	Solubility limit (mol%)	Phase change and melting point	Effect of addition of oxide on sintering characteristics of nanopowder
CGO	Ce^{4+}	111	–	–	–
Fe_2O_3	Fe^{3+}	92	<4	Fe_2O_3 1290 °C → Fe_3O_4 1550 °C → melt	Positive
NiO	Ni^{2+}	83	<1	NiO 1990 °C → melt	Negative
CuO	Cu^{2+}	87	<3	CuO 1026 °C → Cu_2O + liquid 1235 °C → melt	Positive
La_2O_3	La^{3+}	130	<4	La_2O_3 2315 °C → Melt	Negative
SrO	Sr^{2+}	140	<4	SrO 2430 °C → melt	Negative
Co_3O_4	Co^{2+}	104	<1	Co_3O_4 900 °C → CoO 1935 °C → melt	Positive

The radii of the cations are used the values in the octahedral site for Ce^{4+}, La^{3+}, Sr^{2+}, Fe^{3+}, and Co^{2+} and the ones in the hexagonal site for Ni^{2+} and Cu^{2+} ions.

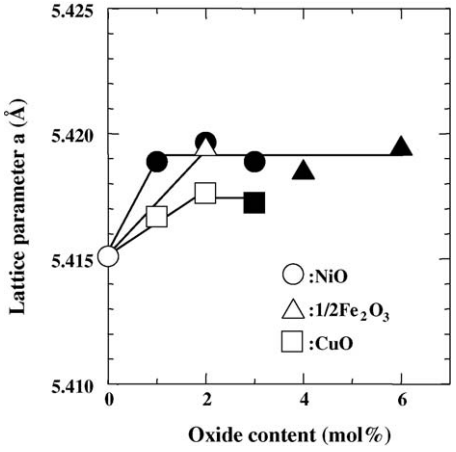

Fig. 1. Lattice parameters of CGO nanopowder heated with the components (NiO, Fe_2O_3 or CuO) in the anode at 1200 °C for 20 h in air, as a function of content of the oxides. The closed symbols show the samples with two phases.

Fig. 2 shows the lattice parameters of CGO nanopowder heated with the components (La_2O_3, SrO or Co_3O_4) in the cathode at 1200 °C for 20 h in air as a function of content of the oxides. The closed symbols represent the samples with two phases. It is reported that $Ce_{1-x}La_xO_{2-\delta}$ solid solution with a single fluorite phase, which was synthesized by the coprecipitation method, is observed for the samples with $x \geq 0.4$ [15]. However, in the case of the solid-state technique, the solubility limit of La_2O_3 into CGO was <4 mol% in this study. For the fluorite oxides, the major difficulty in clarifying the correct solid-state phase relationships arises from fact that the reactions in their systems are relatively slow below 1400 °C [16]. Because several elements can be homogeneously mixed at the atomic level by the coprecipitation method, it is easy to attain the equilibrium condition of lanthanum doped cerium oxides. On the other hand, the components are mixed at the power level by the solid-state technique. Thus, the discrepancy of solubility limit should be explained by the different powder preparations although the parent substances differ. In the case of the $(CGO)_{1-x}(SrO)_x$ system, the lattice parameter of the CGO increased remarkably with increasing SrO content and $SrCeO_3$ perovskite as a second phase was observed in the region of $x \geq 4$ mol%. No reaction products were observed for the mixture of CGO and Co_3O_4, and the solubility limit of $1/3Co_3O_4$ into CGO was <1 mol%.

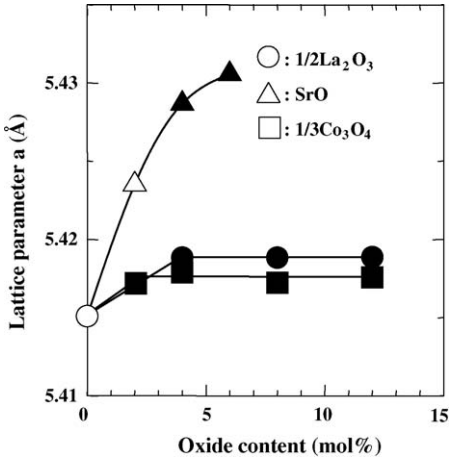

Fig. 2. Lattice parameters of CGO nanopowder heated with the components (La_2O_3, SrO or Co_3O_4) in the cathode at 1200 °C for 20 h in air, as a function of content of the oxides. The closed symbols show the samples with two phases.

It was found that the effect of the components on sintering of CGO electrolyte was strongly affected by the components. The phase changes of the oxides and the effects of addition of the oxides on sintering of the CGO are summarized in Table 1. By addition of Fe_2O_3, Co_3O_4 and CuO to CGO, remarkable enhancement of the sintering characteristics was observed. In contrast, addition of La_2O_3, SrO and NiO notably inhibited an increase of the sintered density.

Figs. 3–5 show the effect of Fe_2O_3, Co_3O_4 and CuO addition on the density of sintered CGO as a function of holding time at (a) 900 °C and (b) 1000 °C, where the closed symbols represent the samples with relative densities greater than 96%. The broken lines show the relative density of the pure CGO. The relative density changes are presented as the circles for the CGO with 0.5 mol% oxide, the triangles for the CGO with 1 mol% oxide and the squares for the CGO sample with 2 mol% oxide. The positive effect of oxide addition on sintering characteristics of CGO has a tendency to increase with increasing content of the oxide, heating temperature, and holding time at the temperatures. In particular, addition of CuO showed the highest effect on sintering characteristics, and the CGO with 2 mol% CuO reached to be greater than 96% density even at 900 °C for 20 h.

Note that the CGO powder synthesized by the conventional coprecipitation method also showed a similar improvement of

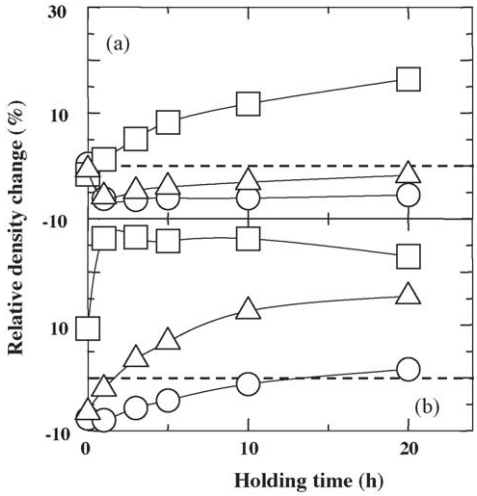

Fig. 3. Effect of Fe_2O_3 addition on the density of sintered $Ce_{0.9}Gd_{0.1}O_{1.95}$ as a function of holding time at 900 and 1000 °C. The relative density changes are presented as the circles for the CGO with 0.5 mol% oxide, the triangles for the CGO with 1 mol% oxide and the squares for the CGO sample with 2 mol% oxide.

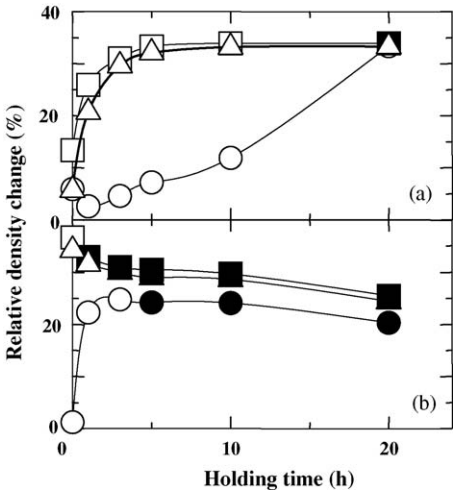

Fig. 5. Effect of CuO addition on the density of sintered $Ce_{0.9}Gd_{0.1}O_{1.95}$ as a function of holding time at 900 and 1000 °C. The closed symbols represent the samples with a relative density ≥96%. For the closed symbols, see the caption in Fig. 3.

sintering characteristics by addition of Fe_2O_3, Co_3O_4 and CuO. This improvement, however, was much smaller when compared to that of the CGO nanopowder synthesized by the new coprecipitation method. On the other hand, no improvement of sintering characteristics was observed for the CGO powder synthesized by the solid-state technique. The BET specific surface area is 31.5 $m^2\,g^{-1}$ for the nanopowder by the new coprecipitation method, 20.1 $m^2\,g^{-1}$ for the fine powder by the conventional one and 1.8 $m^2\,g^{-1}$ for the coarse powder by the solid-state technique. It, thus, was concluded that the effect of oxide addition on the sintering characteristics of CGO showed a tendency to increase with increasing the specific surface area of CGO, namely, with decreasing the particle size of CGO.

In practice, an effect of the cathode material on sintering characteristics of CGO electrolyte is also important. $La_{0.6}Sr_{0.4}CoO_3$ perovskite is well known to be one of the appropriate composition for a cathode of the intermediate-temperature SOFC [10]. Using this material as a starting material, it is tried to confirm it experimentally. In the case of the mixture of the CGO nanopowder and $La_{0.6}Sr_{0.4}CoO_3$, enhancement of sintering characteristics of the CGO was observed at temperatures greater than 1000 °C, and after heating at 1200 °C for 20 h no reaction products were detected by the XRD analysis. Although both elements of La and Sr show the negative effect on sintering of CGO, the positive effect of Co element in the perovskite is dominant during the sintering process of CGO.

It is quite interesting to note why there is a difference in sintering behavior among the CGO with the oxides. Fig. 6 shows the DTA curves of the mixture of CGO nanopowder and 2 mol% $FeO_{1.5}$, and $(CGO)_{0.98}(FeO_{1.5})_{0.02}$ during the heating and cooling process. The sample of $(CGO)_{0.98}(FeO_{1.5})_{0.02}$ are prepared at 1000 °C for 20 h. In the case of the mixture of CGO and

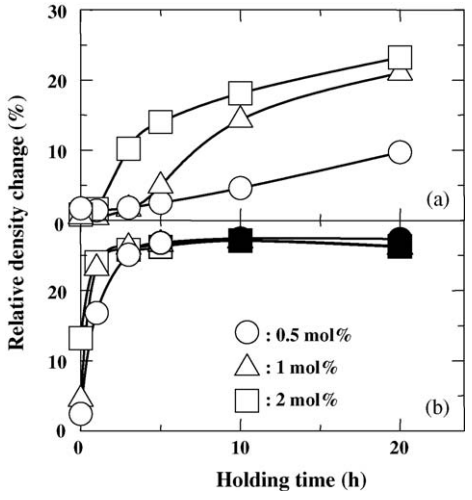

Fig. 4. Effect of Co_3O_4 addition on the density of sintered $Ce_{0.9}Gd_{0.1}O_{1.95}$ as a function of holding time at 900 and 1000 °C. The closed symbols represent the samples with a relative density ≥96%. For the closed symbols, see the caption in Fig. 3.

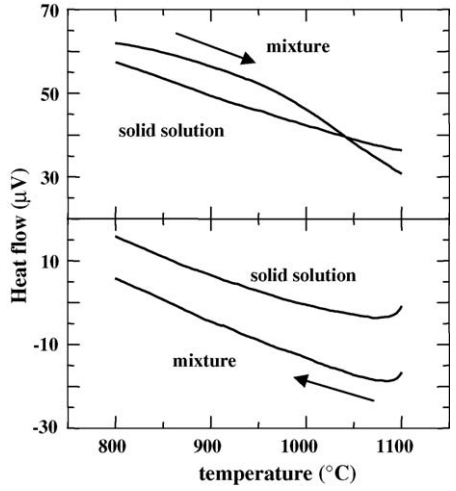

Fig. 6. DTA curves of the mixture of CGO and 2 mol% $FeO_{1.5}$, and $(CGO)_{0.98}(FeO_{1.5})_{0.02}$.

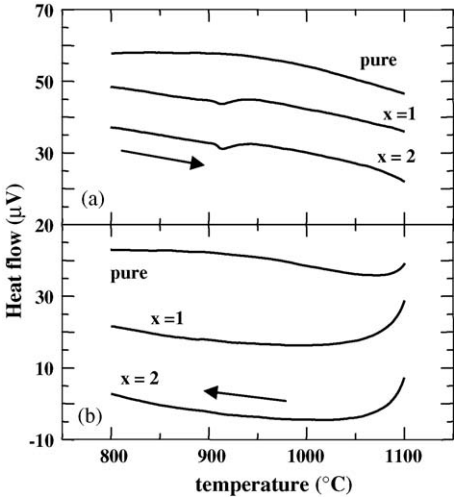

Fig. 7. DTA curves of pure CGO, and the mixture of CGO and Co_3O_4.

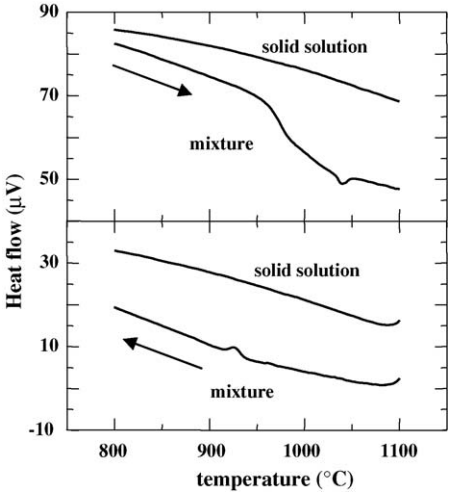

Fig. 8. DTA curves of the mixture of CGO and CuO, and $(CGO)_{0.98}(CuO)_{0.02}$.

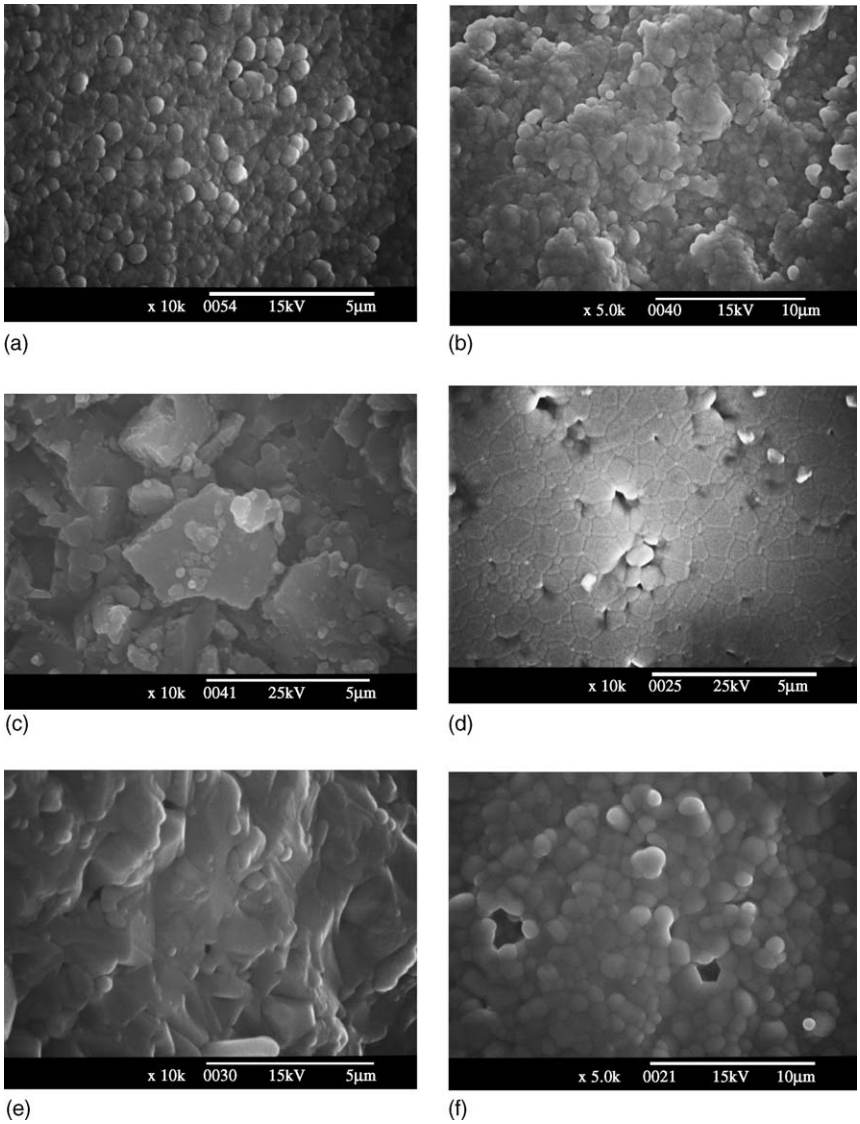

Fig. 9. SEM micrographs of CGO samples by addition of 2 mol% oxides after heating at 1000 °C for 20 h. (a) and (b) CGO with 2 mol% Fe_2O_3; (c) and (d) CGO with 2 mol% Co_3O_4; (e) and (f) CGO with 2 mol% CuO. (a) Cross section; (b) surface section; (c) cross section; (d) surface section; (e) cross section; (f) surface section.

Fe_2O_3, although a slope of the DTA curve slightly changed at approximately 950 °C during the heating process, no changes were seen in the curve during the cooling process. This should be related to a solid-state reaction of the CGO and Fe_2O_3. On the other hand, no remarkable peaks in the DTA curves were observed for the $(CGO)_{0.98}(FeO_{1.5})_{0.02}$ sample.

Fig. 7 shows the DTA curves of pure CGO nanopowder, and the mixture of the CGO and Co_3O_4. Although no peaks in the curve were observed for pure CGO, an endothermic peak n the curve was observed at 908 °C for the CGO with Co_3O_4 during the heating process. Because oxygen release was observed at approximately 908 °C in the TG curve, the endothermic peak in the DTA curve would show the phase change from Co_3O_4 into CoO [17]. During the cooling process, the peak of the phase change from CoO into Co_3O_4 was observed at approximately 798 °C. Additionally, at this temperature the oxygen absorption of the sample with Co_3O_4 was observed by the TG measurement.

Fig. 8 shows the DTA curves of the mixture of CGO and CuO, and $(CGO)_{0.98}(CuO)_{0.02}$. The sample of $(CGO)_{0.98}(CuO)_{0.02}$ are prepared at 900 °C for 20 h. The mixture of CGO and CuO showed a slight change of the DTA slope and its temperature was at approximately 1004 °C for 1 mol% CuO and at approximately 960 °C for 2 mol% CuO addition during the heating process. Additionally, an endothermic peak was observed at approximately 1030 °C during the heating process, and this peak should correspond to the phase change from CuO into Cu_2O and liquid phase [17]. This oxygen release was also observed in the TG measurement. During the cooling process, an exothermic peak of the phase change from Cu_2O and liquid phase into CuO was observed at 936 °C. No peaks in the DTA curves during the heating and cooling process were observed for the $(CGO)_{0.98}(CuO)_{0.02}$ sample.

Fig. 9 shows the SEM micrographs of CGO samples with addition of 2 mol% oxides after heating at 1000 °C for 20 h. The microstructure of CGO sample with Fe_2O_3 consisted of small grain sizes of 0.5–1 μm and shape of particles was round. Clear grain-boundaries were observed. This feature suggests that the densification of the CGO sample with Fe_2O_3 proceeds through the solid-state sintering mechanism. For the CGO sample with Co_3O_4, the microstructure consisted of various grain sizes. It is observed that some grains grew greater than 5 μm and the particles were quite angular. The microstructure of CGO sample with CuO consisted of grain sizes of 1–2 μm. This sample has obscure grain-boundaries, which are probably due to non-crystalline substances. This feature of the microstructure is usually seen in the ceramics sintered by the liquid-phase sintering mechanism. This liquid-phase sintering can be explained by the fact that the phase change from CuO into Cu_2O and liquid phase at approximately 1030 °C.

Fig. 10 shows the shrinkage ratio of vertical to horizontal direction for tablet samples after heating at 900 and 1000 °C as a function of holding time. The content of oxide addition was 2 mol%. The solid-lines represent the shrinkage ratio of pure CGO and the value shows to be approximately one. This shrinkage ratio indicates that sintering of pure CGO must proceed by a bulk ionic diffusion mechanism [18,19]. On the other hand, the shrinkage ratio of the CGO sample with CuO at 1000 °C

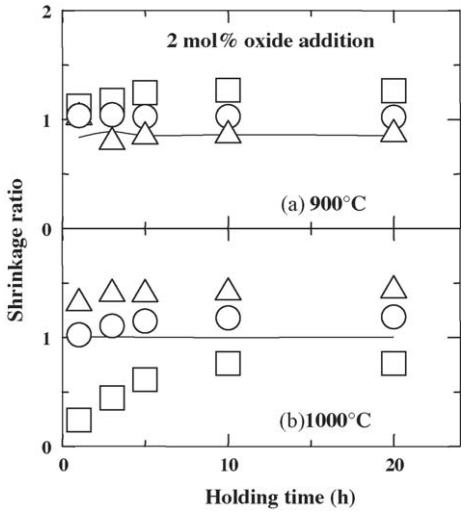

Fig. 10. Shrinkage ratio of vertical to horizontal direction for tablet samples after heating at 900 and 1000 °C as a function of holding time. The solid-lines show the shrinkage ratio of pure CGO. The shrinkage ratio is presented as the circles for the CGO with 2 mol% $FeO_{1.5}$, the triangles for the CGO with 2 mol% ($1/3Co_3O_4$), and the squares for the CGO with 2 mol% CuO.

increased with increasing holding time and approached one. The densification of this material should proceed by a liquid-phase sintering mechanism. After Cu_2O, liquid phase and the CGO should form the solid-solution of $(CGO)_{1-x}(CuO)_x$, this material might proceed by a solid-state sintering mechanism. On the other hand, no remarkable changes in the shrinkage ratio curve were seen in the samples with Co and Fe oxides.

Cobalt oxides are known as sintering aids from experience [20]. One of the reasons is that cobalt oxides easily form the reaction products with a low-temperature melting point although cobalt oxides have a high-temperature melting point [21]. Additionally, the vapor from cobalt oxides promotes the sintering characteristics of materials [22,23]. In the case of CGO with Co_3O_4, the sintering process does not relate to reaction products and liquid phases. Since the vapor of cobalt oxides was observed even at about 900 °C, the samples of CGO with Co_3O_4 included large grains, which seem to relate to cobalt vapor from the cobalt oxide particles. On the other hand, it is thought for the CGO with iron oxides that the low-temperature melting point of iron oxides, namely high ionic bond might be related to the promotion of densification [24]. After the iron oxide makes a solid-solution with CGO, the ionic bond in the CGO should increase. Thus, the $(CGO)_{1-x}(FeO_{1.5})_x$ solid-solution might show the higher sintering characteristics, compared to that of the pure CGO nanopowder.

4. Conclusion

In this study, we clarified the solubility limits for components in the anode and the cathode of the intermediate-temperature SOFC into CGO nanopowder. It was found that a small amount of additions of Fe_2O_3, Co_3O_4 and CuO remarkably enhanced the sintering characteristics of the CGO nanopowder. It was confirmed using the mixture of the CGO electrolyte

and $La_{0.6}Sr_{0.4}CoO_3$ cathode that enhancement of sintering characteristics of the CGO and no reaction products were observed. From these results, it was demonstrated that the CGO nanopowder, which has been developed using the new coprecipitation method, shows the low chemical reaction with the electrodes of the intermediate-temperature SOFC as well as the high sintering characteristics.

Acknowledgements

This work is supported by the Regional New Consortium Projects/Regional New Industry Creative-Type Technology R&D Promotion Programs. The authors would like to thank Shikoku Bureau of Economy, Trade & Industry.

References

[1] B.C.H. Steele, Solid State Ionics 129 (2000) 95.
[2] D.C. Fee, S.A. Zwick, J.P. Ackerman, Proceedings of the High Temperature Solid Oxide Electrolytes, vol. 1, 1983, p. 27.
[3] B.K. Flandermeyer, J.T. Dusek, P.E. Backburn, D.W. Dees, C.C. McPheeters, R.B. Poeppel, Proceedings of the Abstract of National Fuel Cell Seminar, Tucson, Arizona, 1986, p. 86.
[4] F. Nada, S. Komine, M. Kurumada, K. Furuya, Proceedings of the Abstract of the 13th Symposium on Solid Oxide Fuel Cells, Japan, 2004, p. 158.
[5] M.J. Verkerk, A.J.A. Winnubst, A.J. Burggraaf, J. Mater. Sci. 17 (1982) 3113.
[6] K.C. Redford, R.J. Bratton, J. Mater. Sci. 14 (1979) 59.
[7] Y. Takeda, Y. Sakaki, T. Ichikawa, N. Imanishi, O. Yamamoto, M. Mori, N. Mori, T. Abe, Solid State Ionics 72 (1994) 257.
[8] H. Yokokawa, N. Sakai, T. Kawada, M. Dokiya, Denki Kagaku 57 (8) (1989) 829.
[9] E. Suda, B. Pacaud, Y. Montardi, M. Mori, M. Ozawa, Y. Takeda, Electrochemistry 71 (10) (2003) 866.
[10] T. Kawada, K. Masuda, J. Suzuki, A. Kaimai, K. Kawamura, Y. Nigara, J. Mizusaki, H. Yugami, H. Arashi, N. Sakai, H. Yokokawa, Solid State Ionics 121 (1999) 271.
[11] X. Zhang, S. Ohara, H. Okawa, R. Maric, T. Fukui, Solid State Ionics 139 (2001) 145.
[12] A. Ringuede, J.A. Labrincha, J.R. Frande, Solid State Ionics 141–142 (2001) 549.
[13] R. Cracium, S. Park, R.J. Gorte, J.M. Vohs, C. Wang, W.L. Worrell, J. Electrichem. Soc. 146 (1999) 4019.
[14] M. Mori, M. Yoshikawa, H. Itoh, T. Abe, J. Am. Ceram. Soc 77 (8) (1994) 2219.
[15] E. Suda, B. Pacaud, M. Mori, Proceedings of the Rare Earths '04, Nara, Japan, 2004, p. 71.
[16] V.S. Stubican, R.C. Hlnk, S.P. Ray, J. Am. Ceram. Soc. 61 (1–2) (1978) 18.
[17] S. Mizushima, Encyclopadia Chimica, Ktoritsu-Shuppan, 1960.
[18] W.D. Kingery, J. Pappis, M.E. Doty, D.C. Hill, J. Am. Ceram. Soc. 42 (8) (1952).
[19] M. Mori, N. Sakai, T. Kawada, H. Yokokawa, M. Dokiya, Denki Kagaku 59 (4) (1990) 314.
[20] H. Yoshida, K. Miura, J. Fujita, T. Inagaki, J. Am. Ceram. Soc. 82 (1999) 219.
[21] R. Koc, H.U. Anderson, J. Eur. Ceram. Soc. 15 (1995) 867.
[22] R. Koc, H.U. Anderson, J. Eur. Ceram. Soc. 9 (1992) 285.
[23] M. Mori, N.M. Sammes, Solid State Ionics 146 (2002) 301.
[24] W.J. Moore, Physical Chemistry, Longman, Essex, UK, 1972.